A01-3

Model Construction for Computational Anatomy: Progress Overview FY2012

Hiroshi Fujita [#1], Takeshi Hara [#1], Xiangrong Zhou [#1], Chisako Muramatsu [#1], Naoki Kamiya [#2], Min Zhang [#1], Daisuke Fukuoka [#3], Yuji Hatanaka [#4], Tomoko Matsubara [#5], Atsushi Teramoto [#6], Yoshikazu Uchiyama [#7], Huayue Chen [#8], and Hiroaki Hoshi [#9]

[#1] *Department of Intelligent Image Information, Division of Regeneration and Advanced Medical Sciences, Graduate School of Medicine, Gifu University, Gifu-shi, 501-1194 Japan*
[1] `{fujita,hara,zxr,chisa,min}@fjt.info.gifu-u.ac.jp`

[#2] *Department of Information and Computer Engineering, Toyota National College of Technology, 2-1 Eiseicho, Toyota, Aichi, 471-8525 Japan*
[2] `n-kamiya@toyota-ct.ac.jp`

[#3] *Department of Technology Education, Faculty of Education, Gifu University, Gifu-shi, 501-1193 Japan*
[3] `dfukuoka@gifu-u.ac.jp`

[#4] *Department of Electronic Systems Engineering, School of Engineering, the University of Shiga Prefecture, Hassaka-cho 2500, Hikone-shi, Shiga 522-8533, Japan*
[4] `hatanaka.y@usp.ac.jp`

[#5] *Department of Information and Media Studies, Faculty of Information and Media Studies, Nagoya Bunri University, Maeda-365 Inazawacho Inazawa-shi, Aichi 492-8520 Japan*
[5] `matsubara.tomoko@nagoya-bunri.ac.jp`

[#6] *Faculty of Radiological Technology, School of Health Sciences, Fujita Health University, Toyoake-city, 470-1192 Japan*
[6] `teramoto@fujita-hu.ac.jp`

[#7] *Department of Medical Physics, Faculty of Life Science, Kumamoto University, 4-24-1 Kuhonji, Kumamoto-shi, 862-0976, Japan*
[7] `y_uchi@kumamoto-u.ac.jp`

[#8] *Department of Anatomy, Graduate School of Medicine, Gifu University, Gifu-shi, 501-1194 Japan*
[8] `huayue@gifu-u.ac.jp`

[#9] *Department of Radiology, Graduate School of Medicine, Gifu University, Gifu-shi, 501-1194 Japan*
[9] `hoshi@cc.gifu-u.ac.jp`

Abstract— **This paper describes the purpose and summary of our recent progress in the research work, which is a part of research project "Computational anatomy for computer-aided diagnosis and therapy: Frontiers of medical image sciences" funded by Grant-in-Aid for Scientific Research on Innovative Areas, MEXT, Japan. The main purpose of our research in this project is to be engaged in model construction of computational anatomy and CAD applications for automatically recognizing the anatomical structures and analyzing the functions of different organs in whole body region based on different image modalities such as X-ray CT images, MR images, FDG-PET images, eye fundus photographs and dental panoramic radiographs. In the 4th year (2012.4-2013.3, FY2012) of this project, five progresses in anatomical model construction and nine progresses in CAD developments have been achieved. These progresses show the efficiency and potential usefulness of the proposed research works by the promising results.**

I. INTRODUCTION

Modern imaging devices represented by CT, MRI, and PET have been widely used in clinical medicine. The high performance of such scanners can provide detailed information of the whole body region, not only showing real anatomical structures of the patient in 3D, but also being able to visualize the functions of the inner organs within a short time. Therefore, these medical images have been regarded as an important reference for screening, precise diagnosis, and surgery purposes in clinical medicine.

A 3D volumetric image typically includes a large number of axial slices. For example, a torso CT scan generally generates 800-1200 2D axial slices and causes a lot of interpretation burdens for radiologists. Computer-aided diagnosis (CAD) can help to reduce such burden and assist image interpretation [1]. In addition, torso CT images are very suitable for an advanced CAD system that aims at multi-disease detection from multi-organ [2]. In order to realize the aim of the multi-disease detection from multi-organ regions, automatic segmentation/recognition of the detailed anatomical structures and constructing the model of the normal human body are necessary, but it is a still challenging issue. As one of the solutions, modelling the human anatomy and function for normal and abnormal human bodies based on large number of medical images is expected as one of the key techniques [3].

In our previous research works [4], we developed a system to recognize the anatomical structures in torso CT images automatically and try to construct a normal human body model for detecting the abnormality in CT images. However, we found that the robustness and accuracy of this system was not high enough especially for abnormal CT cases that have a large distortion in anatomical structures; generally, these distortions were caused by existing lesion(s). Automated recognition of human anatomy and organ/tissue segmentations in CT images are still challenging issues that have been unsolved by previous research works.

II. RECENT ACHIEVEMENTS

Following our research plan as 4th year (2012.4-2013.3, FY2012), our research activities have been focused on the novel developments and improvements of the previous works in two research topics; one is the anatomical model construction and the other is CAD applications. Fourteen research subjects (five in model construction and nine in CAD application) have proceeded. The overview and relationship of these subjects are shown in Figure 1. The progress of each research subject is described in the following section by comparing with the previous results.
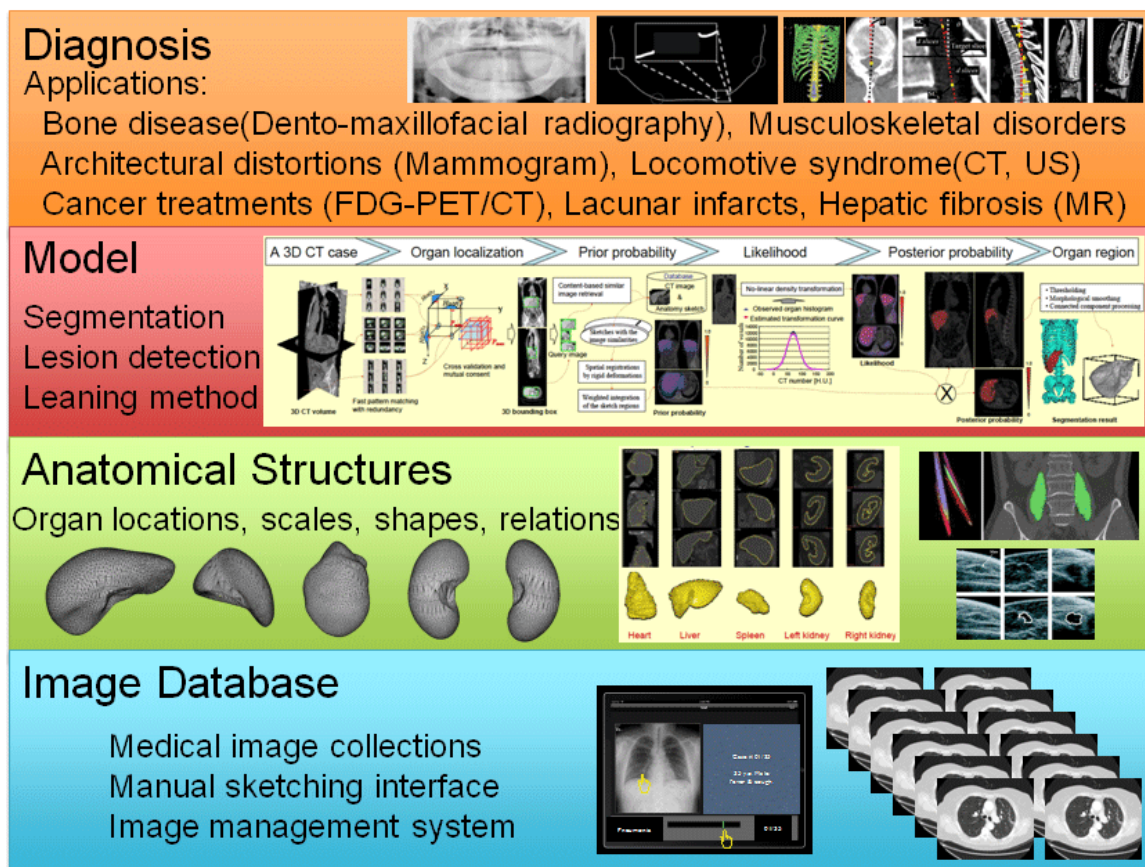

Fig. 1 Overview of our achievements

Purpose: The aim of this research subject is to develop a universal approach that can be used to automatically segment the different massive organ regions on CT images. The traditional approaches for developing automatic segmentation algorithms put the interests on how to generate an ad-hoc method to extract the specific organ-appearance on CT images by the human designers. A common model that can show the anatomical structures of all organs should be constructed firstly and then used to provide the prior knowledge for guiding the segmentation task. However, generating such a model to present all the possible anatomical structures in both normal and abnormal CT cases is difficult and sometimes unrealistic, especially in the case that only a limited number of CT images are known during the development. Therefore, the approach that can learn and update the knowledge of the model directly from database and solve the different organ segmentation problems simply and straightforwardly is expected.

Overview of the approach: In previous works, we have proposed a new approach [5-7] to simplify the organ segmentation process by finding its location in CT images, searching the image patterns that are similar to the inputted image in a database, and transferring the anatomical structures in the selected image patterns directly to the inputted image as the references to guide the segmentation. The proposed approach was fully based on machine-learning and data-driven methods that use more image data instead of complex algorithms to enhance the robustness and accuracy of the organ segmentation process.

Methodology and features: The key point of our proposed approach is to simplify the organ segmentation process as a content-based image retrieval and anatomical structure transformation problem. The approach includes three processing steps: (1) automated target organ localization, (2) content-based image retrieval and atlas construction, and (3) atlas-based organ segmentation. Two techniques have been used in this approach; one is fast object localization based on machine-learning [6], and the other is image retrieval by using a phase-correlation registration based on the fast Fourier transform (FFT) [5].

Experiments: A database (DB) that includes 100 cases of 3D volumetric CT cases was used. These CT cases were collected at Gifu University Hospital by two kinds of multi-slice CT scanners (LightSpeed Ultra16 of GE Healthcare and Brilliance 64 of Philips Medical Systems). The heart, liver, spleen, left kidney, and right kidney were selected as the segmentation targets for evaluating the performance of the proposed approach. One of the authors manually extracted liver region in 38 CT cases, spleen region in 60 CT cases, left kidney in 93 CT cases, and right kidney in 35 CT cases. These regions were used as the ground truth for accuracy evaluation. A leave-one-out cross validation was employed in the experiment. The experimental results showed that proposed scheme can solve the segmentations of the five different inner organs by using one algorithm.

Results: We confirmed that these five target organs were segmented automatically and correctly in all CT cases. The average coincidence ratios determined by the JSC values were 0.67 for heart, 0.78 for spleen, 0.83 for liver, 0.77 for right kidney, and 0.73 for left kidney. It was indicated that our proposed method was very robust for different organ segmentations in both normal and abnormal CT cases. The segmentation results were comparable to the manual inputs of the human operators.

What's new: We got the following three progresses in the 4th year [8-12].

(1) *Improving the robustness and accuracy for automatic organ localization* [8,9]. The key point of this improvement is to introduce the new features for machine-learning approach and use pre-defined organ atlas to validate the location results. Comparing to the Haar-features that were used in previous works; we added the local binary patters (LBP) as main features to distinguish the location of a target organ for both learning and testing processes. The new system was applied to localize the 11 kinds of organs from more than 1,000 CT cases. An example of the localization results was shown in Figure. 2. We confirmed that LBP has more discriminative power for the organ localization task on CT images than Haar-features.

The experimental results showed that the detector based on LBP provided a better performance on accuracy than using Haar-features. These two kinds of features can also complement each other under the proposed localization approach. The results are shown in Figure 2.

(2) *Improving the accuracy of the content-based image retrieval* [10]. We developed a GPU-based number of local patched and calculate the pair-wised patch-image-similarity to increase the specificity of the retrieval process to select the images with the similar appearance around the organ contours. The preliminary experiment showed the potential possibility of the new method to search the images that have the similar organ shapes in DB. However, the difficulties have been
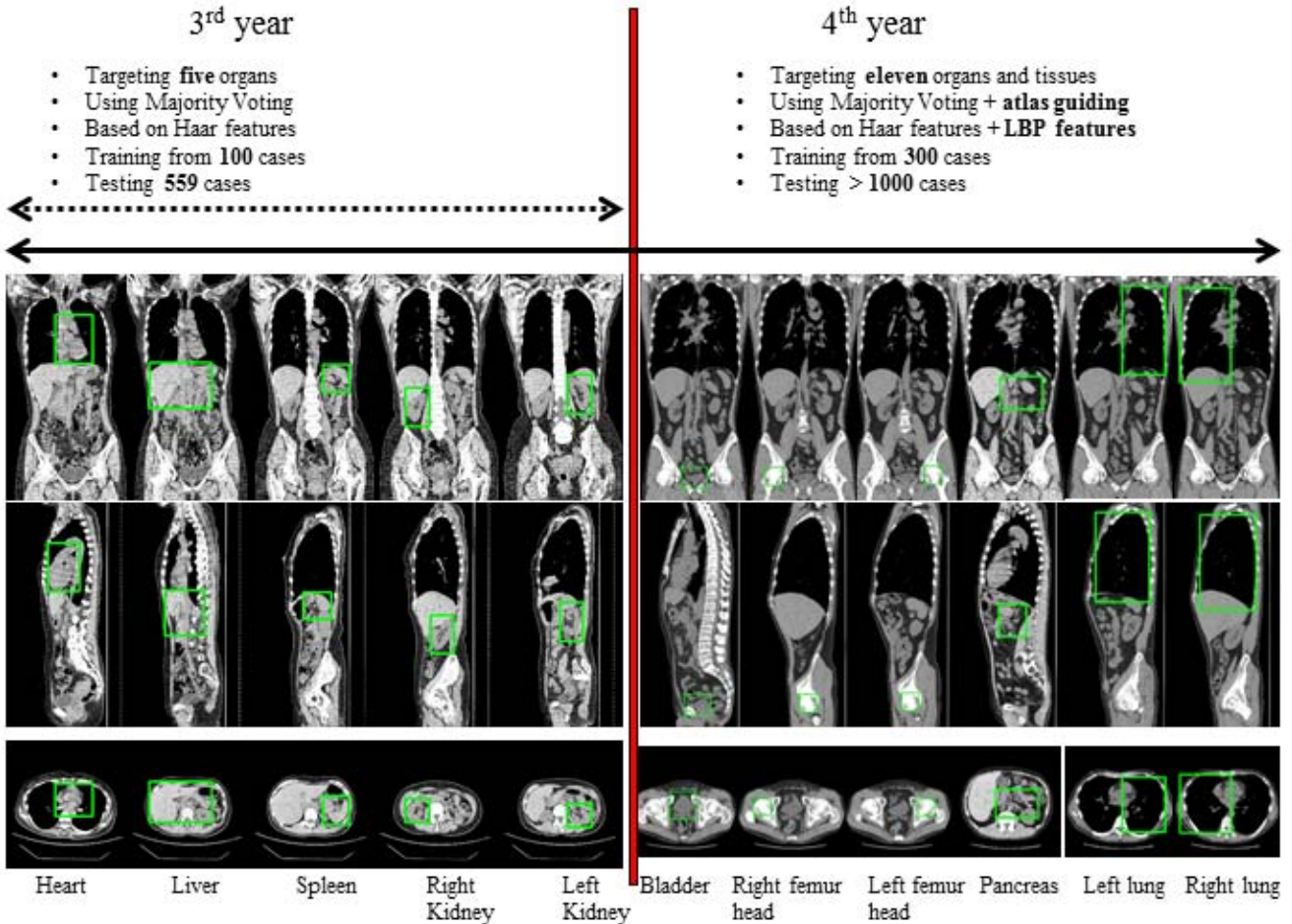

Fig. 2 An example of organs and tissues localization results (Green box indicates the detected target location from three different views).

parallel algorithm to accomplish the image retrieval task. The experiments showed that the new algorithm was ten times faster than the previous one to provide the same outputs. We also tried to improve the image-similarity measuring during the image retrieval to catch the partial image-similarity around the organ contours. Comparing to the previous works that used the global image region to calculate the image correlations between two CT cases; we divided the whole image region into a still remained in patch generation and selections from the CT images. Those problems will be solved in the future works.

(3) *Constructing the database of anatomical structures in torso region based on CT images* [11,12]. In previous works, we have constructed an image database that includes thousands of torso CT cases. This time, we aim to get the anatomical structures from the CT images and construct a database to store the anatomical structures of the

human torso regions. The anatomical structures have been defined as the positions of bounding box and the contour information of the inner organs in a CT case. We manually inputted such information for liver and spleen regions in 300 CT cases by 8 operators. The accuracy, variance and time cost of the manual inputs from the different operators were evaluated. The experimental results showed that our working-flow for constructing the anatomical structure database worked well.

Conclusion: we proposed an universal scheme for the segmentation of different organ regions automatically in 3D CT cases. Machine-learning-based organ localization, content-based image retrieval, and atlas-based organ segmentation techniques have been combined in this scheme to accomplish segmentation for the different organ regions by using the same algorithm. In 4th year, we approved this system and applied to localize 11 kinds of organ regions in more than 1000 CT cases, and its efficiency and accuracy were shown in the results. This scheme can be used for the anatomical structure database construction for understanding and computing the human anatomy based on medical images.

B. A Model-based approach to recognize abdominal muscle region in CT images [13-16]

Purpose: In our previous work, anatomical shape model has been proposed and applied to the psoas major muscle and the rectus abdominis muscle. The model-based approach was effective for segmenting the muscle region with characteristic shape. However, in order to achieve rectus abdominis muscle segmentation based on the model, it must consider the variations of the body. In FY 2012, we applied it to additional test cases for recognizing muscle region. The result was reported in [13] and [14]. Moreover, we made improvement on the recognition method of the rectus abdominis muscle based on generating a virtually projected image and a shape model for the rectus abdominis muscle in [15] and [16].

Methods overview: Firstly, in order to simplify the body structure, we proposed a new method with virtually projected image that is to unfold virtually a 3-D human body to a 2-D plane (Fig. 3) [15]. It

has been integrated into an automated recognition for rectus abdominis muscle.

Secondly, to take into account the body difference on the virtually unfolded image, we improved the generating method of virtually unfolded image by the removal of subcutaneous fat region which is widely different between patients. The new method for generating the virtually unfolded image was proposed to simplify the body
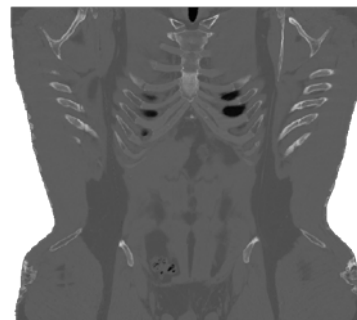

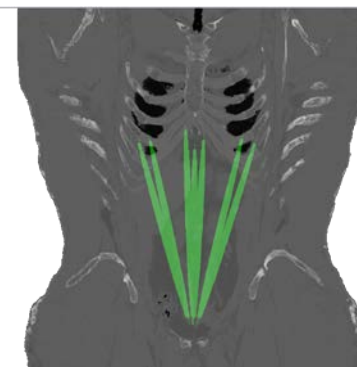Fig. 3 Slice image of virtually unfolded image

Fig. 4 Anatomical centerline on the virtually unfolded image

Fig. 5 Recognition result of rectus abdominis muscle

difference and to raise robustness of the anatomical feature recognition on the images. In Figure 4, green lines indicate the muscle fiber direction generated by the recognized landmarks. Finally the muscle region was recognized on the image using this model, which was indicated by the area, including all muscle fiber lines. Figure 5 shows the recognition result of rectus abdominis muscle. In conclusion, for the muscle recognition of the abdominal regions with large body differences, the virtually unfolded image is effective to simplify the body variations. It suggests the possibility of an application of this method to the other muscle recognitions.

What's new: (1) Increase in the test cases and confirmation on the effectiveness of the model-based approach for rectus abdominis muscle recognition. (2) Improvement of segmentation performance of the rectus abdominis muscle by use of the virtually unfolded image, which was newly proposed in FY 2012.

C. FDG-PET: Temporal subtraction for cancer treatments[17-19]

Purpose: Diagnostic imaging on FDG-PET scans was often used to evaluate chemotherapy results of cancer patients. Radiologists compare the changes of lesions' activities between previous and current examinations for the evaluation. The progress of this year was to show the fundamental usefulness of the computerized detection and tracking system of abnormal spots based on an observer performance study.

Methods overview: Z-score mapping based on statistical image analysis was applied to the temporal subtraction technique. The subtraction images can be obtained based on the anatomical standardization results because all of the patients' scans were deformed into standard body shape[17]. An observer study was performed without and with CAD to evaluate the usefulness of the scheme by ROC (receiver operating characteristics) analysis. Readers were asked to set their confidence levels from absolutely no change to definitely change between two scan on a continuous scale[18,19].

Results: The recognition performance for the 43 pairs was 96% sensitivity with 31.1 false-positive marks per scan. The average of area-under-the-ROC-curve (AUC) from 4 readers was increased from 0.85 without CAD to 0.90 with CAD (p=0.0389, DBM-MRMC) as shown in Figure 6. The average of interpretation time was decreased from 42.11 to 40.04 seconds per case (p=0.625, Wilcoxon test). Figure 7 shows an example that the computer output was beneficial for readers.

We concluded that the CAD system for torso FDG-PET scans with temporal subtraction technique might improve the diagnostic accuracy of radiologist for cancer therapy evaluation.

What's new: (1) we applied PET/CT to constructing FDG model instead of only PET scans. (2) Observer performance study was performed to obtain the fundamental usefulness of proposed CAD scheme.
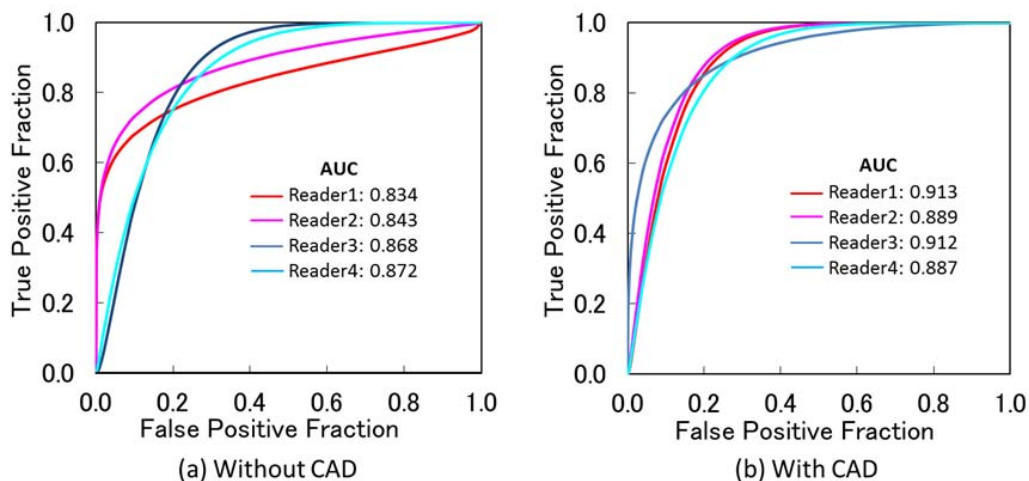

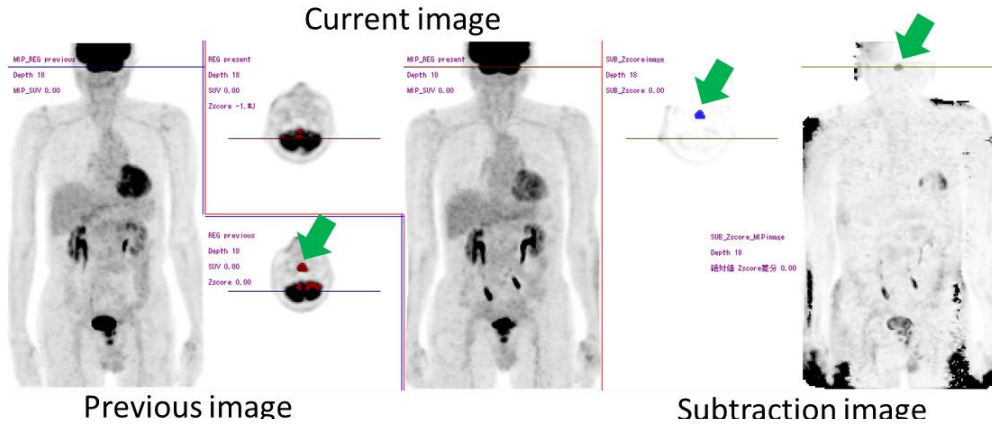Fig.6 ROC curves for 4 readers in case of without (a) and with (b) CAD.

Fig.7 CAD beneficial case. Green arrow indicates an abnormal spot.

D. Pulmonary emphysema classification based on texton learning model by sparse representation[24,25]

Purpose: Chronic obstructive pulmonary disease (COPD) is a disease of pulmonary system and is a growing health problem worldwide. Emphysema is one of important kinds of COPD. The three described morphological types of emphysema are centrilobular emphysema (CLE), panlobular emphysema(PLE) and paraseptal emphysema (PSE). Computerized classification and quantification of this disease is very important. Texture classification method based on local binary patterns (LBP) and texton learning with k-means have been introduced for the classification and quantification of COPD recently [20-22]. In our previous work [23], we used a texture classification method based on textons learned via sparse representation in the classification of emphysema. This method is inspired by the great success of l_1-norm minimization based sparse representation (SR). The dictionary of textons is learned by applying SR to image patches in the training dataset. The SR coefficients of the test images over the dictionary are used to construct the histograms for texture classification. Textons learned in dictionary learning stage are not sensitive to intensity difference. When dealing with CT images, intensity is of a physical property of the tissue which may be related to pathological pattern. Hence, intensity information should be included in the feature histogram. In this work, 3D joint SR-coefficient-and-intensity histogram maps are proposed as the features used in the classification of emphysema.

The joint SR coefficients and intensity histogram map capture information about at which intensity levels the different textons reside.

Overview of the approach: The proposed approach mainly includes four stages[24,25]. The details of the proposed method are as follows.

(1) ROI preprocessing

The test images were obtained from 14 different subjects, including 6 PSE subjects, 5 CLE subjects and 3 PLE subjects of different stages. Totally 470 regions of interest (ROIs) were extracted from these subjects.

(2) Texton learning by K-SVD

a) Before texton learning, all training ROI images are normalized to have zero mean and unit standard deviation. Hence, for each type of ROIs, a training dataset $X = [x_1, x_2, \cdots, x_n]$ is constructed, where $x_i, i = 1, 2, \cdots, n$ is the patch vector at a position in a training sample image of this type. The dictionary of textons, denoted by $D = [d_1, d_2, \cdots, d_k]$, can be learned from the constructed training dataset X, where $d_j, j = 1, 2, \cdots, k$, is one of the k textons. In this stage, a high-pass filter is applied to exclude the patches reside in smooth regions.

b) Then an overcomplete dictionary of textons is learned by optimizing D and $d_j, j = 1, 2, \cdots, k$ of the function below by using K-SVD [26]

$$\arg \min_{D, \Lambda} = \| X - D\Lambda \|_F^2 + \lambda \| \Lambda \|_0,$$

where $\Lambda = [\alpha_1, \alpha_2, ..., \alpha_n]$ is the SR objective function. In this stage, orthogonal matching pursuit (OMP) is used to update the dictionary.

(3) Feature extraction

New 3D joint SR coefficients and intensity histogram maps are used. The joint SR coefficients and intensity histogram captures information about at which intensity levels the different textons reside to improve discrimination results.

(4) ROI classification

Finally, the ROI image can be classified to the corresponding class by the selected classifier using the proposed feature histograms.

Results: The proposed scheme was applied to 14 patient cases of non-contrast CT images (Table 1). Each CT image covers the whole torso region with an isotopic spatial resolution of 0.63 mm and a 12 bits density resolution. In the experiments, a training set is constructed only by 47 ROIs, which account for about 10 % of the total ROIs, for the subjects with different emphysema.

The performance of the proposed approach is summarized in Tables 2 and 3. The confusion matric in Table 3 shows that the proposed method generally agrees on the class labels.

What's new: In FY 2012, a new 3D joint SR coefficients and intensity histogram maps are proposed in the classification of emphysema based on the texton learning via sparse representation. Preliminary experimental results on large quantity of images, including various stages of emphysema, validate the usefulness of the proposed method.

TABLE 1 DETAILS OF TEST DATASET.

	Number of ROIs	Size of ROI
PSE	167 (6 subjects)	
CLE	240 (5 subjects)	40×40
PLE	63 (3 subjects)	

TABLE 2 THE AVERAGE PERFORMANCE FOR DIFFERENT TYPES OF EMPHYSEMA CLASSIFICATION.

Average accuracy	PSE	CLE	PLE
Proposed	73.6	87.5	88.9

TABLE 3 CONFUSION MATRIC SHOWING THE TRUE LABLE VS. LABLE ASSIGNED BY THE CLASSIFIER FOR THE PROPOSED METHOD.

		True labels		
Proposed method	Estimated labels	PSE	CLE	PLE
	PSE	123	25	2
	CLE	38	210	5
	PLE	6	5	56

E. Automated measurement of mandibular cortical width on dental panoramic radiographs by using mandibular contour model[27,28]

Purpose: Clinical studies have shown that the mandibular cortical width (MCW) measured on dental panoramic radiographs (DPRs) is significantly correlated with bone mineral density (BMD) in the hip, lumbar spine and femoral neck. Therefore, identifying asymptomatic patients with osteoporosis through dental examinations may bring a supplemental benefit to the patients. However, most DPRs are used only for diagnosing dental conditions by dentists in their routine clinical work, and the condition of the mandibular cortex is generally not paid attention.

What's new: We have developed a CAD scheme that automatically measures MCW to assist dentists in screening osteoporosis [27]. In FY2012, we have analysed some of the results from our second multi-clinic trials, and made some modification to our previous methods to improve robustness. We evaluated our scheme on 100 DPRs, including 26 osteoporotic cases, by a leave-one-out test method, and the result has been published in [28].

Overview of the approach: The overview of our MCW measurement method is illustrated in Fig.8. First, potential mandibular edges were detected by use of a mandibular mask and a modified Canny edge detector. The most similar mandibular contour model was selected from the training cases by the similarity score based on the distance transformation. The selected model was used as the initial model and fitted to the test case by active contour method. The mental foramina positions of the fitted model, which were identified manually beforehand, were determined as the MCW measurement positions. Finally, the upper margins of the cortices were determined by the profile analysis.

Results: The relationship between MCW measurements by a dental radiologist and the experimental result is shown in Fig.9. There was a relatively good agreement between the two, with the correlation coefficient of 0.84. The areas under the receiver operating characteristic curves were 0.96 and 0.98 for the automatic and manual measurements, respectively.
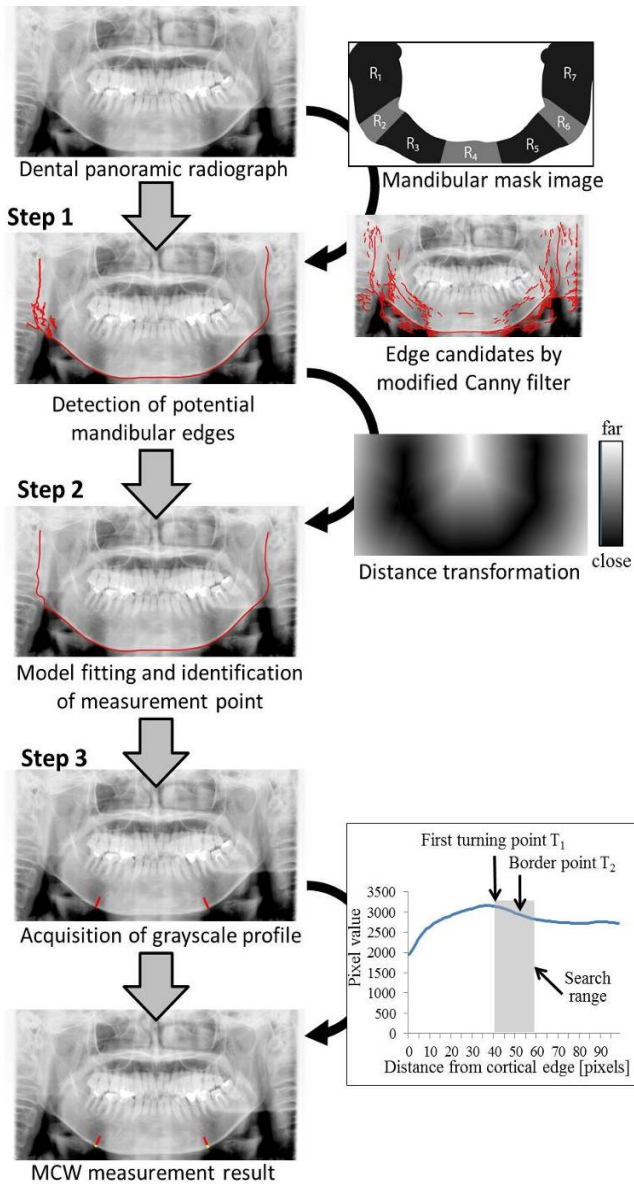
Fig.8. Overview of the automated MCW measurement scheme.

With the threshold of 2.7 mm, the sensitivity and specificity were 88.5% and 97.3%, respectively, by the automatic measurement.

In the second multi-clinic trials, 6 dental clinics have participated, and most cases from 5 clinics have been checked by the dental radiologist. Out of 275 cases, 13 cases were considered suspected osteoporosis. By use of our method, the sensitivity was 84.6% while the specificity was 82.8%. These suspected cases are likely unidentified in the routine dental examinations. The results indicate the potential utility of our CAD system for early diagnosis of osteoporosis.
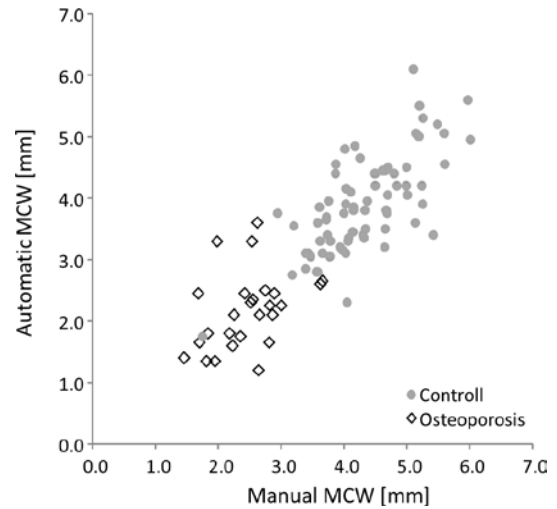

Fig. 9. The relationship between the MCW measurements by the dental radiologist and the proposed method.

III. RECENT ACHIEVEMENTS (CAD APPLICATION)

A. *Improvement of brain CAD scheme for classification of lacunar infarcts and enlarged Virchow Robin spaces using Visible Korean Human Image*

Purpose: The detection of lacunar infarcts is important because their presence indicates an increased risk of severe cerebral infarction. Therefore, we developed a CAD scheme for the detection of lacunar infarcts (Fig.10) [29]. A retrospective observer study was also carried out to evaluate the performance of radiologists in detecting lacunar infarcts on T_1-and T_2-weighted images without and with use of the CAD scheme. For all nine radiologists, the mean area under the ROC curves without and with computer output were 0.89 and 0.93, respectively.

In the observer study, we realized that the majority of FPs detected by the computer are different from those detected by radiologists, and radiologists can therefore disregard these obvious FPs identified by computer. However, it is of interest to note that some FPs due to enlarged Virchow-Robin spaces detected by the computer were difficult for radiologists to distinguish from lacunar infarcts. These FPs were the main sources to the detrimental effects of the CAD scheme. A strong influence on radiologists by these FPs might result in unnecessary medical treatment for the patient.

Lacunar infarcts were often detected in basal ganglion, optic thalamus, and cerebral deep white matter. Whereas, enlarged Virchow-Robin spaces were symmetrically detected in the lower third of basal ganglion. Therefore, anatomical location must be useful features for distinguishing between them. Therefore, we improved our CAD scheme for classification of lacunar infarcts and enlarged Virchow-Robin spaces by using anatomical location features.

Methods overview: Our database consisted of T_1- and T_2-weighted images obtained from 109 patients, which included 89 lacunar infarcts and 20 enlarged Virchow-Robin spaces. First, we enhanced the lesion in T_2-weighted image by using the white top-hat transformation. A gray-level thresholding was subsequently applied to the enhanced image for the segmentation of lesion. For measuring shape features, we determined size, irregularity and signal intensities in T_1- and T_2-weighted images. To obtain anatomical locations, we employed an image registration technique, in which Visible Korean Human Image was used as a reference image. Finally, a neural network was employed for distinguishing between lacunar infarcts and enlarged Virchow-Robin spaces.

Results: The results indicated that the area under ROC curve increased from 0.89 (without location features) to 0.93 (with location features).

What's new: (1) We improved our CAD scheme by using anatomical location features, and (2) Visible Korea Human Image was used to obtain the anatomical location features.
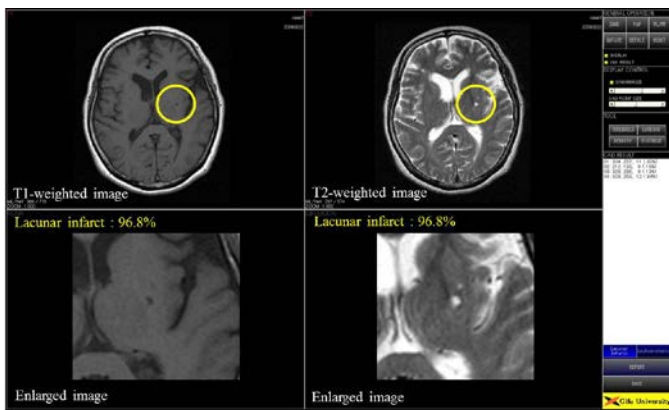

Fig. 10. Illustration of a prototype CAD scheme for the detection of lacunar infarct.

B. Investigation of probabilistic models for localization of optic disc on retinal fundus images

Background: Retinal fundus photography is frequently and widely used examination for diagnostic record, longitudinal comparison, and screening of eye diseases. Because it can visualize blood vessels non-invasively, it is sometimes imaged during health check-ups. In reading retinal fundus images, physicians must look for various signs of abnormalities. However, the number of qualified professional is limited, and reading many screening images is time consuming. Therefore, for reducing physicians' workloads and improving diagnostic efficiency, we have been investigating the computerized diagnosis and quantification systems for glaucoma, diabetic retinopathy, and
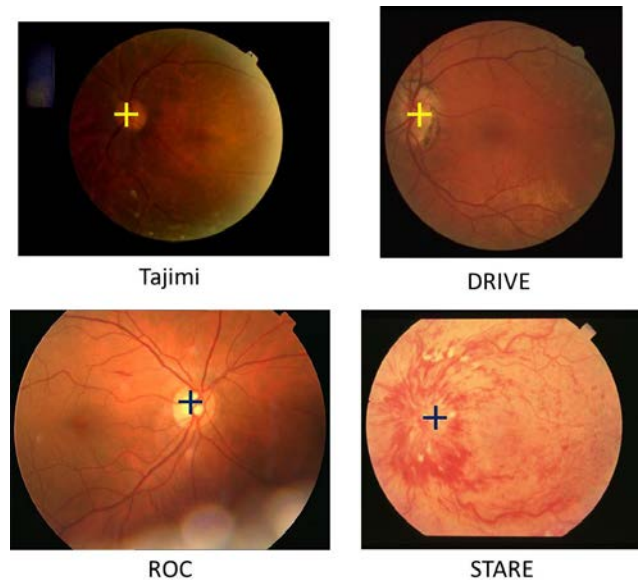

Fig. 11. Examples of succeeded optic disc detection results

hypertensive retinopathy.

In processing the images, it is important to first identify or segment normal structures, such as optic disc, fovea, and blood vessels, because they are the targets of measurement, can serve as landmarks, and are occasionally the sources of false positives. A number of groups have been investigating automated methods for detection and segmentation of optic disc. We have also previously developed automatic detection and segmentation schemes [30]. The detection scheme was based on the facts that optic discs are generally bright and have oval shapes. However, when there is a bright

abnormality or when the exposure is uneven, the previous method may fail to detect the optic disc.

What's new: To improve detection accuracy without decreasing time efficiency, we have investigated a new scheme by using the probabilistic models. To our knowledge, no groups have investigated a model-based disc detection scheme.

Materials and Methods: Using training cases, we created two models, namely, intensity model and vessel likelihood model, by averaging the intensity images and vessel detection images, respectively, after registration. For registration, affine transformation is applied using manually specified disc location. For applying the models, main vessels for a test case were detected, and the vessel scores were determined by shifting and multiplying the result image to the vessel likelihood model. At the pixel with the highest score, the local matching was performed with the intensity model to refine the location.

Results: The method was tested with four databases, including three public databases [31-33] and Tajimi Database [34]. As the result, the successful detection rates were 100% in Tajimi Database (162/162 cases) and ROC Database (100/100 cases), 97.5% in DRIVE Database (39/40), and 77% in STARE Database (62/81 cases). For STARE cases, our method succeeded in 29 of 31 (94%) cases of normal eyes. Figure 11 shows examples of succeeded detection results. In STARE database, there are several cases in which optic discs are partially visible in the images. In such cases and cases in which large abnormalities present, the vessel detection result by our present method was insufficient, and the method failed to detect optic discs correctly. Compared with our previous intensity-based method, the detection rate was improved by the new method. However, the further improvement is necessary.

C. Hybrid detection method of pulmonary nodules using PET/CT images

Purpose: Lung cancer is the leading cause of death among men worldwide. To reduce the number of cancer-related deaths, early detection and treatment of the cancer are essential. PET/CT is an imaging technique that provides functional and anatomical information; it is useful for the early detection of lung cancer. Typically, radiologists examine a large number of images, and reducing the radiologists' workload is highly desirable. The purpose of this study was to develop an automated scheme for detecting pulmonary nodules in PET/CT images using combined detection.

Methods overview: The initial nodule candidates were detected from both CT [35] and PET images. False positives (FPs) were then eliminated in the initial candidates by using support vector machine with characteristic values obtained from CT and PET images.
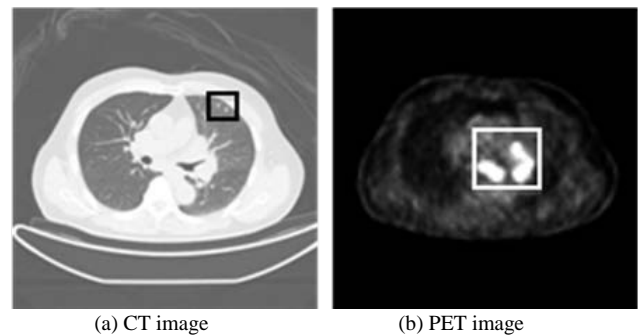

(a) CT image   (b) PET image

Fig.12 Automated detection results. (a) and (b) are the axial images at the same slice position. Boxes indicate the nodules detected by the proposed method.

Results: Figure 12 shows the result that nodules were detected correctly. In Figure 12(a), two isolated nodules were seen in CT image; proposed method detected the nodule using CT image. In Figure 12(b), highly uptake regions adhered to the mediastinum were detected in PET image. Thus, it was shown that complemented detection was performed using both PET and CT images. We evaluated the true-positive fraction (TPF) and the number of FPs/case using 100 cases. The sensitivity was 83.2% with the number of FPs/case at 5.0; it was more than 10% higher than that of independent detection systems using only CT or PET images [36].

What's new: (1) Improvement of detection performance by hybrid FP reduction using three support vector machines and characteristic features obtained by two modalities. (2) Constructing about 100 cases of PET/CT image database. These images

were acquired using a PET/CT scanner during a cancer-screening program.

D. Determination of similarity measures using multidimensional scaling and linear regression models for selection of reference breast mass images

Purpose: Mammography is considered an effective screening tool for breast cancer. When an abnormality is found, physicians make a pathologic inference and compare the findings with those by other imaging modalities. However, diagnosis of mammograms can be challenging, especially for novice readers. We have previously proposed a computer-aided diagnosis system which provides similar reference images for classification of benign and malignant masses on mammograms [37-39].

What's new: In current study, we investigated a new method based on the multidimensional scaling (MDS) for determining similarity of breast masses [40,41]. The MDS has been primarily used for visualization purposes. In the medical imaging field, there has not been a study that attempted to utilize MDS for image retrieval.

Methods: MDS [42] is a technique often used for visualization which can map dissimilarity or distance data as a geometrical picture. Using this technique, we attempted to figure out the spatial relationship representing the similarities between breast masses by using subjective similarity data obtained by experts, and to reproduce the space using feature values. For applying MDS, subjective similarity (dissimilarity) data for sample cases were obtained from 8 experts in mammography reading. As a preliminary investigation, we considered 9 pathologic types, and selected 3 samples from each type which required 351 similarity data by each expert. The average similarities were used for MDS analysis, and each dimension in MDS configuration was fitted by the linear combination of 13 image features with a least square error.

Results: Figure 13 shows the MDS configuration of the first and second dimensions in 4D map. The MDS map shows the similarity relationship between different pathologic masses, such that cysts and fibroadenomas are generally considered very similar, scirrhous carcinomas and invasive lobular carcinomas are considered similar, and mucinous

carcinomas can include those that are similar to malignant types and others that are similar to
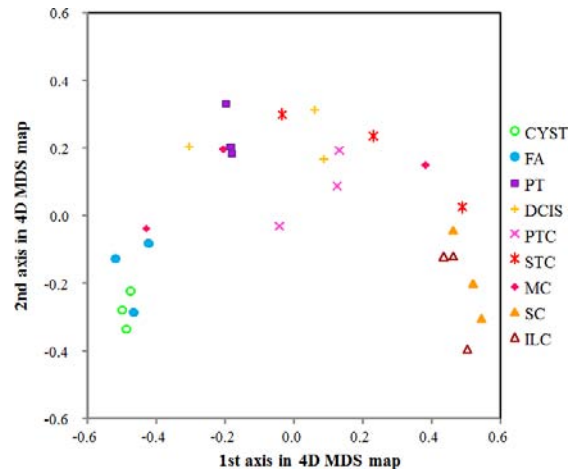

Fig. 13. MDS configuration of the 1st and 2nd dimensions in 4D map. FA: fibroadenoma, PT: phyllodes tumor, DCIS: ductal carcinoma in situ, PTC: papillotubular carcinoma, STC: solid-tubular carcinoma, MC: mucinous carcinoma, SC: scirrhous carcinoma, ILC: invasive lobular carcinoma.
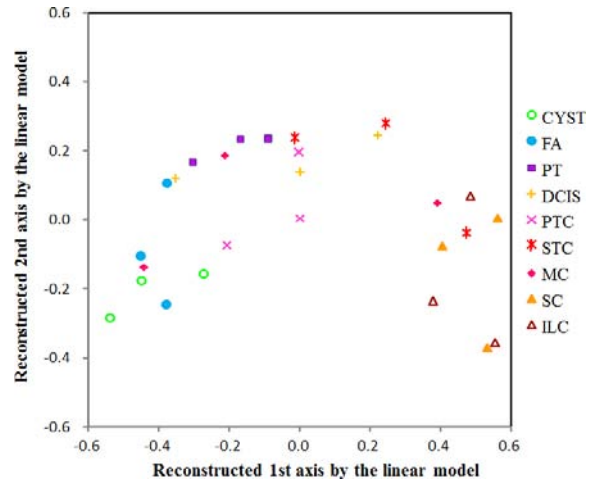

Fig. 14. The fitted map by the linear combination of image features

benign types. The reconstructed map by use of the linear combinations of features is shown in Fig.14. By using the features, the similarity map was reproduced relatively well. When dissimilarity measures were determined by the distance in the reconstructed map, the correlation between the subjective similarity ratings and the dissimilarity measures was -0.87. The correlation was higher than that for the dissimilarity measures based on the distance in conventional feature space (-0.65). The result indicates the potential usefulness of the proposed scheme. However, the method must be tested with a larger test set.

E. Automated detection of architectural distortion in mammogram using adaptive Gabor filter
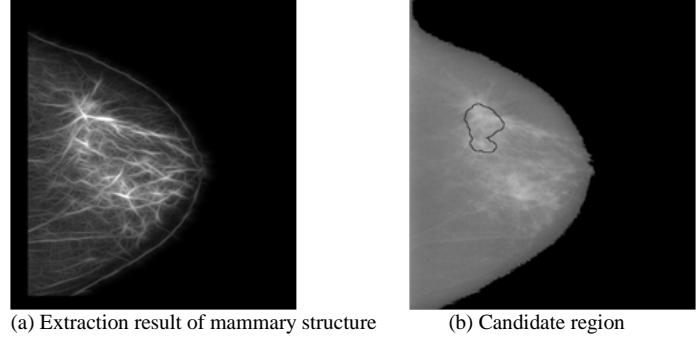
Purpose: Architectural distortion is the most missed findings in screening mammogram. Furthermore, there is challenge regarding the automated detection of the architectural distortion about the sensitivity. The aim of this study was to develop a novel automated method for detecting architectural distortion.

Methods overview: This method consists of the analysis of the mammary gland structure, detection of the distorted region, and reduction of false positive results. We developed the adaptive Gabor filter for analysing the mammary gland structure in which filter parameters were determined depending on the thickness of the gland structure [43,44]. The distorted region of the mammary gland was then detected as an initial candidate using a concentration index followed by binarization and labelling. False positives in the initial candidates were eliminated using a support vector machine with 23 characteristic features [45].

Experiments: In the experiments, we compared the automated detection results with interpretations by a radiologist using 50 cases (200 images) obtained from the Digital Database of Screening Mammography (DDSM).

The resulting true positive rate was 81.0%, and the number of false positive per image was 1.4. These results indicate that the proposed method may be useful for detecting architectural distortion in mammograms (Fig.15).

What's new: We developed the adaptive Gabor filter for analyzing the mammary gland structure in which filter parameters were determined depending on the thickness of the gland structure. Performance of filter was better than conventional Gabor filter.

(a) Extraction result of mammary structure   (b) Candidate region

Fig.15 The output images obtained by the proposed method.

F. Mammography CAD for architectural distortion

Purpose: We have been developing an automated method for detecting spiculated architectural distortions on mammograms. The method consists of three steps: i) extraction of mammary gland by

(a)   (b)
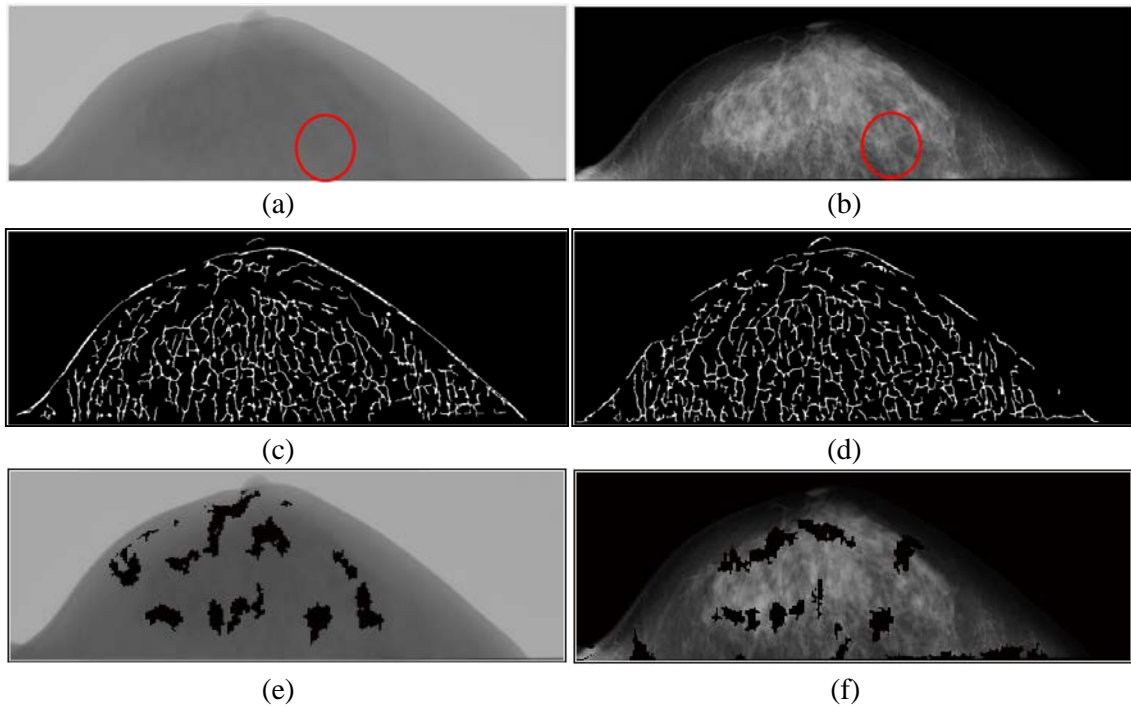
(c)   (d)

(e)   (f)

Fig. 16 Two kinds of mammograms are detected processing images. (a) For-Processing image. (b) For-Presentation image. The circles in (a) and (b) show the sites of architectural distortions. (c) and (d) are extracted liner structures in (a) and (b), respectively. (e) and (f) are detected candidate areas at initial pick-up stage in (a) and (b), respectively.

normal curvature, ii) extraction of distorted area by concentration index and isotropic index, and iii) elimination of false positives (FPs).

Our present researches are to compare the results of our detection method on two kinds of mammograms [46] and to reduce FPs using assessment of fibroglandular breast tissue density [47].

Methods overview: (1) *Comparison of automated detection performance of architectural distortion on two kinds of mammograms*

We examined the application of our detection method to digital mammograms. In digital mammography, there are two kinds of images (Fig. 16). One is "For-Processing" image, which is an original digital mammogram. The other one is "For-Presentation" image, which is processed for interpretation that resembles analog mammograms in appearance. The results show that the performances both at the first pick-up stage and at the FP elimination stage on For-Presentation images are higher than ones on For-Processing images.

(2) *Reduction of FPs using assessment of fibroglandular breast tissue density*

Mammographic density is highly individual because of the consequence of fatty involution of mammary gland with relation to increased ages. Our assessment method consists of two steps; i) division of breast region into three regions according to density, ii) classification of mammograms into four categories (i.e., fatty, mammary gland diffuseness, non-uniform high density, and high density) based on the rate of each of three regions. Although the threshold value of elimination of FPs by pixel value was a fixed value in our previous method, it is a variable value according to the categories in our new method. A new feature calculated based on the pixel values of divided three regions is added the other features for elimination of FPs using discriminant analysis. As a result, it is possible to reduce more FPs by the new method than the previous method.

What's new: (1) Effectiveness of application of the developed detection algorithm to For-Presentation Image. (2) Improvement of FP elimination technique using assessment of fibroglandular breast tissue density.

G. Preliminary investigation on CAD system update: Effect of selection of new cases on classifier performance

Background: Computerized medical image analysis has been studied in broad topics with various image modalities and diseases, some of which have already been employed in practice or may be employed in the future. When CAD system is implemented in clinical practice, it would be desirable that the system is constantly updated with some improvement based on the mistakes. Because clinical cases are continuously accumulated after the installation of the system, an effective use of these cases should be considered for improving the performance. In some cases, it may be preferable to reduce the number of training cases for reducing the time of retraining and workload, if user input is required, or to remove outliers that may degrade the system performance. In this study, as a preliminary study, we investigated the effect of different case selection methods in updating three types of classifiers for a task of distinguishing benign and malignant breast masses on mammograms [48].

Methods: Three classifiers used in this study were linear discriminant analysis (LDA), support vector machine (SVM), and k-nearest neighbors (kNN). For simplicity, the image features used in the 3 classifiers were fixed, including the effective diameter, circularity, elliptical irregularity, edge contrast, full-width at half-maximum of modified radial gradient histogram and radial gradient index, which were used in the previous study [49]. For SVM, a radial basis function kernel was used. For kNN, two tests were performed with a constant parameter k of 13 and a variable parameter k, which was set to 6% of the number of training cases. The database of masses were obtained from the Digital Database for Screening Mammography [50], and consisted of 728 malignant and 840 benign masses.

For investigating the effect of case selection methods, a simulation study was conducted by randomly sampling the training and test datasets. A schematic diagram for the sampling procedure is shown in Fig.17. First, evaluation dataset E was sampled without replacement to keep them independent of the training cases. From the remaining, an initial training dataset I was sampled with replacement and used for the baseline classifier. At each update, dataset T was sampled

for intermediate testing and retraining. They were tested by the current classifier, and some of them were selected (dataset S) to be added to the training set on the basis of the test result. The updates were repeated 10 times, and the initial classifier and the classifier at each update were evaluated by the evaluation dataset E. The whole procedure was performed 100 times to reduce the sampling effect. The numbers of cases in E and T were set to 200 cases including 100 benign and 100 malignant masses. The number of cases in I was varied between 200, 400 and 600, whereas that in S was varied between 10, 20, and 40.

Four case selection methods were evaluated: (a) selection of most correctly classified cases, (b) selection of most incorrectly classified cases, (c) selection of indeterminate cases, and (d) random selection. For comparison, inclusion of all cases was also tested, although the number of training cases would become about 3 to 7 times larger in this scenario. The performance was evaluated by the area under the operating characteristic curves (AUCs).
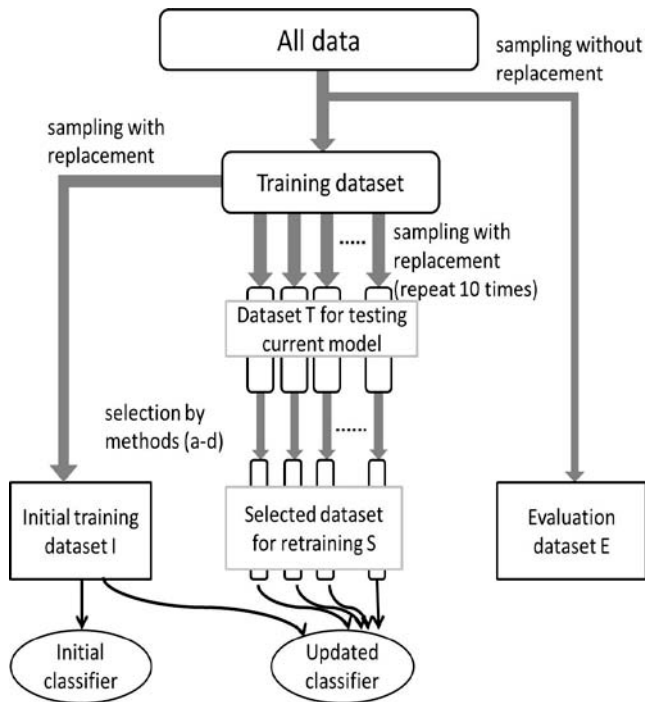

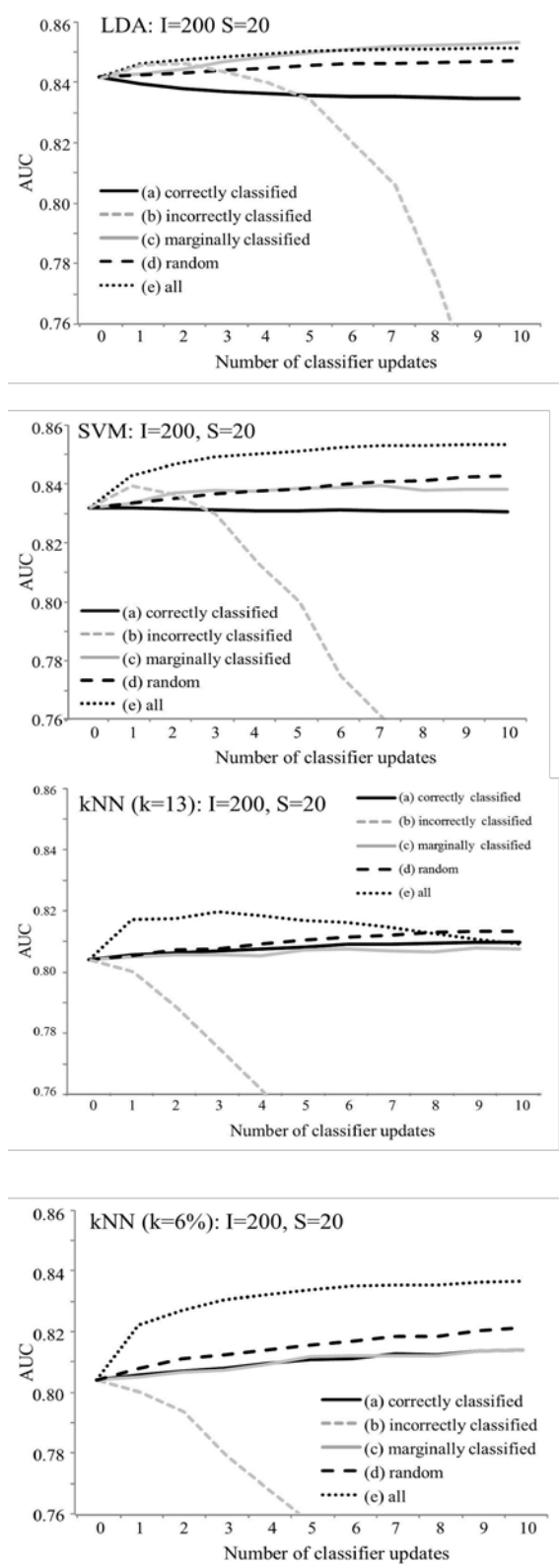Fig. 17. Schematic diagram for the sampling procedure

Fig. 18. Effect of retraining classifiers on average AUCs by the different case selection methods with dataset I of 200 cases and dataset S of 20 cases

Figure 18 shows average AUC after each update by different case selection methods with LDA, SVM, and kNN, when the numbers in I and S were 200 and 20, respectively. The initial AUCs were somewhat lower with kNN, which may be due to the facts that parameter optimization was not sufficient and that the feature set was fixed. Instead of the absolute values, only changes in AUCs were considered in this study. In general, AUCs were almost unchanged with the method (a). With (b), the AUCs slightly improved in the beginning for LDA and SVM but decreased as the updates were repeated. In the cases of the methods (c) and (d), AUCs improved for three classifiers except kNN with constant k. For SVM and kNN with variable k, AUCs by using all cases were significantly higher than those by using selected cases. For LDA, AUCs by the method (c) were comparable with those by using all cases.

Results: When the numbers of cases in I and S were varied, similar trends were observed. However, in the case of LDA, the classification performance by the method (b) became considerably higher when dataset I was large. It was predicted that when the fraction of the incorrectly classified cases was kept small, they can contribute in the improvement of the classifier. In the case of kNN with constant k, different result was observed. When dataset I became large, AUCs stayed almost constant by the methods (a), (c), and (d), while by using all cases, they decreased and became lower than those by the other methods. The result indicated that when the number of nearest neighbors, k, becomes too small

compared to the training dataset, classification performance can be degraded.

Conclusion: We investigated the potential effect of updating CAD system with newly obtained cases for improving the classifiers. As an initial investigation, the effect of different sampling methods on three different classifiers was studied. In general, the classification performances for the models using the marginally classified cases were comparable with those for the models using the randomly selected cases and lower than those for the models using all the cases. In the case of LDA, when the fraction of the additional cases was small, e use of the incorrectly classified cases resulted in a beneficial effect. However, since an optimal fraction of incorrectly classified cases is not known at this time, and the selection of marginally classified cases may require an extra work, use of all cases or randomly classified cases, if case reduction is extremely desirable, is considered the reliable way. Further investigation is certainly needed with different classification tasks and image modalities to draw a strong conclusion.

H. Locomotive syndrome

Background: In recent years, quantitative evaluation of "Locomotive syndrome" caused by musculoskeletal disorders which describe the state of high-risk condition of requiring care is expected. For evaluation of Locomotive syndrome, methods for evaluating pannation angle of the gastrocnemius muscle on ultrasound images have been focused (Fig.19).
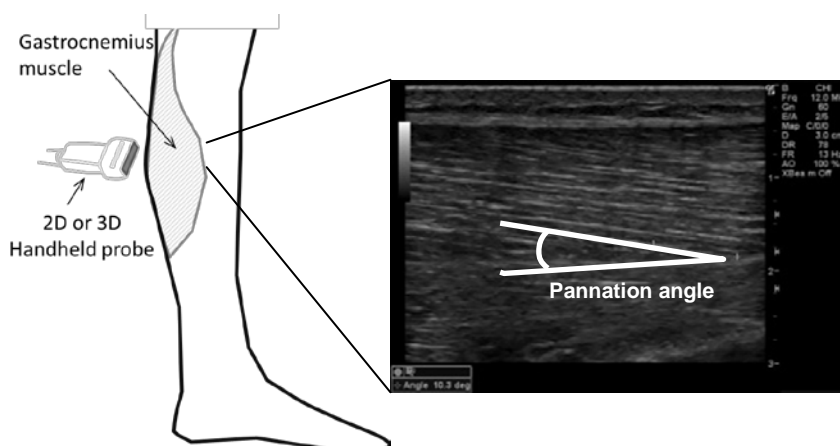

Fig.19 Pannation angle of the gastrocnemius muscle.

Methods: In this study, we developed methods for a quantitative evaluation of the pannation angle on 2D or 3D-ultrasound images. First, we determined the top and bottom aponeurosis by approximation of curvilinear muscle-fiber area. Second, after we extracted muscle fiber from the muscle-fiber area, a high pass filter was applied by Fourier transform and the angle of rotation of principal axis of moment in the limited area was considered as the angle of the muscle fiber. Finally, we calculated the mean angle of a line tangent to the curvilinear surface of the bottom aponeurosis and determined pannation angle by adding the mean angle of the tangential line to the angle of the muscle fiber [51-53].

Results: As a result, the correlation coefficient between the angles measured by this method and by the 2D-ultrasound images was 0.79.

I. Automatic extraction of liver contour for staging hepatic fibrosis on Gd-EOB-DTPA-enhanced MRI images [54]

Purpose: Irregularity of hepatic surface is one of the essential findings on MR images for the diagnosis of fibrosis. Gd-EOB-DTPA is a liver-specific MRI contrast medium, and its hepatocyte-phase images yield excellent hepatic enhancement. Therefore, the objective delineation of hepatic contour morphology would be effectively done using such contrast-enhanced images. We have been working on developing a quantitative evaluation method for staging hepatic fibrosis using hepatic contour information, which is automatically extracted from Gd-EOB-DTPA-enhanced hepatocyte-phase MR images. The average error between the usage of automated contour and manually extracted contour by a radiologist was 0.79 mm. The difference of mean the standard deviations (SDs) of the difference values between the contour and a polynomial approximated curve in the F0-F2 group and F3-F4 group was of statistical significance ($p < 0.05$, Tukey test).

Methods overview: The proposed technique extracts the contour of liver automatically using unsharp-mask filter and p-tile method in the region of interest (ROI) manually determined over the right robe of liver. Figure 20 (a) shows the binary image with p-tile thresholding technique from the ROI image after the unsharp-mask filtering. Figure 20 (b) indicates the maximum area image (white area) of the binary image, which was determined as the liver region. We determined the starting point of contour tracing in which the raster scan finds the first object pixel on the maximum area image. The liver contour of automatic extraction was made by tracing the starting point to bottom of the image. Figure 20 (c) shows the liver contour by our automatic extraction method. The classification for staging hepatic fibrosis is achieved by employing SD.

Results: This study was performed to develop an automatic extraction method of liver contour on Gd-EOB-DTPA-enhanced MRI images. The average error between the automated and manually extracted contours was 0.79 mm. The contours by the proposed method are almost the same as those by manual extraction. In addition, the difference of mean SDs in the F0-F2 group and F3-F4 group was of statistical significance ($p < 0.05$, Tukey test).

What's new: We proposed a new method and conformed that the proposed technique may be useful for quantitative evaluation of fibrosis on Gd-EOB-DTPA-enhanced MR images.

Fig. 20 Image binarization of ROI area to determine the liver region for contour analysis. (a) Binary image with p-tile thresholding technique. (b) Maximum area image for a liver extraction. (c) An example of automatically extracted contour from image in (b).

IV. CONCLUSIONS

Our recent progresses for anatomical model construction and applications based on multimodality medical images were described. According to our research plan for previous year, we improved our universal solution for automatic organ segmentation and confirmed its usefulness and efficiency by applying to 11 kinds of organ regions based on more CT cases. This work is beneficial to the further anatomical model constructions by providing a possible way to extract

a large number of anatomical structures quickly and automatically from the CT images.

We also improved a whole body probabilistic model to show the metabolic activities of the normal organs and tissues based on FDG-PET images. This work showed the potential possibility of our consideration that detecting the lesions by comparing the patient image to a normal human body model. The consideration was proposed by our group for solving the problem of the multi-lesion detection in multi-organs.

Our models have been applied to many CAD systems and confirmed its good performances and usefulness.

Our research group has been collaborated with several research groups of the same research project. Especially, we have been working together with the Kido Lab. of Yamaguchi University, and shared the image database and source codes of the programs each other for shape model constructions. The novel results of these research works have been presented in [12].

As the future works, we will continue the collaboration with the other groups in this research project to accomplish the anatomical model definition, construction, and applications.

REFERENCES

[1] K.Doi: Computer-aided diagnosis in medical imaging: Historical review, current status and future potential, Computerized Medical Imaging and Graphics, Vol.31, 198–211, (2007).

[2] H.Kobatake: Future CAD in multi-dimensional medical images - Project on multi-organ, multi-disease CAD system, Computerized Medical Imaging and Graphics, Vol.31, pp.258–266, (2007).

[3] H.Fujita, T.Hara, X.Zhou, H.Chen, and H.Hoshi: Computational anatomy: Model construction and application for anatomical structures recognition in torso CT images, Proc. of the First International Symposium on the Project "Computational Anatomy", 58-61, (2010).

[4] H.Fujita, T.Hara, X.Zhou, T.Hayashi, N.Kamiya, H.Chen, and H.Hoshi: Model construction for computational anatomy: Progress overview FY2011, Proc. of the 3rd International Symposium on the Project "Computational Anatomy", 24-32, (2012).

[5] X.Zhou, A.Watanabe, X.Zhou, T.Hara, R.Yokoyam, M.Kanematsu, and H.Fujita: Automatic organ segmentation on torso CT images by using content-based image retrieval, Proc. of SPIE Medical Imaging, Vol.8314, 83143E-1 - 83143E-7, (2012).

[6] X.Zhou, S.Wang, H.Chen, T.Hara, R.Yokoyama, M.Kanematsu, H.Hoshi and H.Fujita: Automatic localization of solid organs on 3D CT images by a collaborative majority voting decision based on ensemble learning, Computerized Medical Imaging and Graphics, Vol.36, No.4, 304-313, (2012).

[7] X.Zhou and H.Fujita: Automatic organ localization on X-ray CT images by using ensemble learning techniques, in Machine learning in computer-aided diagnosis: Medical imaging intelligence and analysis, ed. by K.Suzuki, 403-418, IGI Global, USA, (2012).

[8] X.Zhou, A.Yamaguti, X.Zhou, T.Hara, R.Yokoyam, M.Kanematsu, and H.Fujita, "Automatic organ localizations on 3D CT images by using majority-voting of multiple 2D detections based on local binary patterns and Haar-like features," Proc. of SPIE medical imaging, in press, 2013.

[9] A.Watanabe, X.Zhou, T.Hara, R.Yokoyama, M.Kanematsu, and H.Fujita: Automated organ segmentation on CT images by using similar image retrieval based on machine-learning, Radiological Society of North America 2012, LL-INE1194-SUB, (2012).

[10] A.Watanabe, X.Zhou, H.Chen, T.Hara, R.Yokoyama, M.Kanematsu, H.Hoshi, and H.Fujita: Probabilistic atlas construction by using content-based image retrieval from non-contrast CT images, The Japanese Society of Medical Imaging Technology, OP7-10, (2012).

[11] S.Yamaguchi, X.Zhou, H.Chen, T.Hara, H.Jiang, R.Yokoyama, M.Kanematsu, H.Hoshi and H.Fujita, "Investigation on the method of constructing a database of anatomical structures in torso region based on CT images," IEICE Technical Report, Vol.112, No.411, 83-88, (2013).

[12] S.Yamaguchi, X.Zhou, R.Xu, T.Hara, R.Yokoyama, M.Kanematsu, H.Hoshi, S.Kido, and H.Fujita: Construction of statistical shape models of organs in torso CT scans using MDL method, Proc. of International Forum on Medical Imaging in Asia, P2-33, (2012).

[13] N.Kamiya, X.Zhou, J.Kondo, H.Chen, C.Muramatsu, T.Hara, R.Yokoyama, M.Kanematsu, H.Hoshi, and H.Fujita: Fully automated quantitative measurement of multiple skeletal muscles in torso CT images by use of statistical shape models, 98th Scientific Assembly and Annual Meeting of the Radiological Society of North America, Informatics: Scientific Informal (Poster) Presentations, LL-INS-MO5A, (2012).

[14] N.Kamiya, X.Zhou, H.Chen, C.Muramatsu, T.Hara, and H.Fujita: Model-based approach to recognize the rectus abdomens muscle in CT images, IEICE Transactions on Information and Systems, Vol.E-96-D, No.4, in press, (2013).

[15] N.Kamiya, C.Muramatsu, X.Zhou, H.Chen, R.Yokoyama, T.Hara, M.Kanematsu, H.Hoshi, and H. Fujita: Model-based approach to recognize the rectus abdominis muscle in CT images by use of a virtually image-unfolding technique, Proc. of International Forum on Medical Imaging in Asia, 47, (2012).

[16] N.Kamiya, C.Muramatsu, X.Zhou, H.Chen, T.Hara, H.Hoshi, and H.Fujita: Automated recognition of the rectus abdominiss muscle in CT images based on a virtual image-unfolding technique by the removal of the subcutaneous fat region, IEICE Technical Report, Vol.112, No.411, MI2012-99, 197-200, (2013).

[17] Y.Shimizu, T.Suzuki, T.Kobayashi, T.Hara, X.Zhou, S.Ito, S.Kumita, K.Ishihara, T.Katafuchi, and H.Fujita: Evaluation of anatomical registration method for torso FDG-PET scans, IEICE Technical Report, Vol.MI2011-78, 7-10, (2012).

[18] Y.Shimizu, T. Hara, D. Fukuoka, X.Zhou, C.Muramatsu, T.Kobayashi, S.Ito, S.Kumita, K.Ishihara, T.Katafuchi, and H.Fujita: Diagnosis support for cancer trteatment on torso FDG-PET/CT scans by using anatomical standization method, JAMIT, (2012).

[19] Y.Shimizu, T.Hara, D.Fukuoka, X.Zhou, C.Muramatsu, S.Ito, K.Hakozaki, S.Kumita, K.Ishihara, T.Katafuchi, and H.Fujita: Temporal subtraction system on torso FDG-PET scans based on statistical image analysis, Proc. of SPIE Medical Imaging, in press, (2013).

[20] M.Gangeh, L.Sørensen, S.Shaker, M.Kamel, M.de Bruijne, and M.Loog: A texton-based approach for the classification of lung parenchyma in CT images, T.Jiang et al. (eds.), MICCAI 2010, LNCS, Vol. 6363, 596-603, Springer, Heidelberg, (2010).

[21] M.Gangeh, L.Sørensen, S.Shaker, M.Kamel, M.de Bruijne, and M.Loog: Multiple classifier systems in texton-based approach for the classification of CT images of lung, Proc. of the 2010 International MICCAI Conference on Medical computer vision: Recognition techniques and applications in medical imaging. Springer, Heidelberg, (2010)

[22] L.Sørensen, S.B.Shaker, and M.de Bruijne: Texture classification in lung CT using local binary patterns, in MICCAI (1), ser. (Lecture Notes in Computer Science 5241), D.N.Metaxas, L.Axel, G.Fichtinger, and G.Székely, Eds., Springer-Verlag, New York, 934–941, (2008).

[23] M.Zhang, X.Zhou, S.Goshima, H.Chen, C.Muramatsu, T.Hara, R.Yokoyama, M.Kanematsu, and H.Fujita: An application to pulmonary emphysema classification based on model of texton learning by sparse representation, SPIE Medical Imaging Conference, (2012).

[24] M.Zhang, X.Zhou, S.Goshima, H.Chen, C.Muramatsu, T.Hara, R.Yokoyama, M.Kanematsu, and H.Fujita: Computer-aided diagnosis for pulmonary emphysema classification based on texton learning via sparse representation, International Forum on Medical Imaging in Asia, (2012).

[25] M.Zhang, X.Zhou, H.Chen, C.Muramatsu, T.Hara, R.Yokoyama, M.Kanematsu, and H.Fujita: Pulmonary emphysema classification based on an improved texton learning model by sparse representation, Proc. of SPIE Medical Imaging, in press, (2013).

[26] M.Aharon, M.Elad, and A.Bruckstein: The KSVD: An algorithm for designing overcomplete dictionaries for sparse representation, IEEE Trans. Signal Process., Vol. 54, No.11, 4311-4322, (2006).

[27] T.Matsumoto, T.Hayashi, T.Hara, A.Katsumata, C.Muramatsu, X.Zhou, Y.Iida, M.Matsuoka, K.Katagi, and H.Fujita: Automated scheme for measuring mandibular cortical thickness on dental panoramic radiographs for osteoporosis screening, Proc. of SPIE, Vol. 8315, 83152L16, (2012).

[28] C. Muramatsu, T. Matsumoto, T. Hatashi, T. Hara, A. Katsumata, X. Zhou, Y. Iida, M. Matsuoka, T. Wakisaka, and H. Fujita: Automated measurement of mandibular cortical width on dental panoramic radiographs, International Journal of Computer Assisted Radiology and Surgery, 23 Nov., 2012 (online first).

[29] Y.Uchiyama, T.Hara, J.Shiraishi, M.S.Chung, and H.Fujita: Improvement of CAD scheme for classification of lacunar infarcts and enlarged Virchow Robin spaces using Visible Korean Human Image, Proc. of International Forum on Medical Imaging in Asia, O5-2, (2012).

[30] C.Muramatsu, T.Nakagawa, A.Sawada, Y.Hatanaka, T.Yamamoto, and H.Fujita: Automated segmentaion of optic disc region on retinal fundus photographs: Comparison of contour modeling and pixel classification methods, Comput. Methods Programs Biomed., Vol.101, 23-32, (2011)..

[31] J.J.Staal, M.D.Abramoff, M.Niemeijer, M.A.Viergever, and B.van Ginneken: Ridge based vessel segmentation in color images of the retina, IEEE Trans. Medical Imaging, vol. 23, 501-509S, (2004).

[32] M.Neimeijier, B.van Ginneken, M.J.Cree, A.Mizutani, G.Quellec, C.I.Sanchez, B.Zhang, R.Horneero, M.Lamard, C.Muramatsu, X.Wu, G.Cazuguel, J.You, A.Mayo, Q.Li, Y.Hatanaka, B.Cochener, C.Roux, F.Karray, M.Garcia, H.Fujita, and M.D.Abramoff: Retinopathy online challenge: Automatic detection of microaneurysms in digital color fundus photographs, IEEE Trans. Medical Imaging, Vol. 29, 185-195, (2010).

[33] Structured Analysis of the Retina. [Online]. Available: http://www.ces.clemson.edu/~ahoover/stare/

[34] A.Iwase, Y.Suzuki, M.Araie, T.Yamamoto, H.Abe, S.Shirato, Y.Kuwayama, H.K.Mishima, H.Shimizu, G.Tomita, Y.Inoue, and Y.Kitazawa: The prevalence of primary open-angle glaucoma in Japanese. The Tajimi study, Ophthalmol, Vol. 111, 1641-1648, (2004).

[35] A.Teramoto and H.Fujita: Fast nodule detection in chest CT images using cylindrical nodule-enhancement filter, International Journal of Computer Assisted Radiology and Surgery, June 2012 (online first).

[36] A.Teramoto, H.Fujita, K.Takahashi, K.Ozaki, S.Murata, O.Yamamuro, T.Kobayashi, T.Tamaki, and M.Nishio, Development and evaluation of automated nodule detection in lung PET/CT images, International Forum on Medical Imaging in Asia, (2012).

[37] C.Muramatsu, Q.Li, K.Suzuki, R.A.Schmidt, J.Shiraishi, G.M.Newstead, and K.Doi: Investigation of psychophysical measure for evaluation of similar images for mammographic masses: Preliminary results, Medical Physics, Vol. 32, 2295-2304, (2005).

[38] C.Muramatsu, Q.Li, R.A.Schmidt, J.Shiraishi, K.Doi, Investigation of psychophysical similarity measures for selection of similar images in the diagnosis of clustered microcalcifications on mammograms, Med Phys vol. 35, pp. 5695-5702, (2008).

[39] C.Muramatsu, Q.Li, R.A.Schmidt, J.Shiraishi, and K.Doi : Determination of similarity measures for pairs of mass lesions on mammograms by use of BI-RADS lesion descriptors and image features, Academic Radiology, Vol.16, 443-449, (2009).

[40] C.Muramatsu, K.Nishimura, M.Oiwa, M.Shiraiwa, T.Endo, K.Doi, and H.Fujita: Correspondence among subjective and objective similarities and pathologic types of breast masses on digital mammography, IWDM, Springer Lectures Notes in Computer Science (LNCS) series, Vol.7361, 450-457, (2012).

[41] C. Muramatsu, K. Nishimura, T. Endo, M. Oiwa, M. Shiraiwa, K. Doi, and H. Fujita : Representation of lesion similarity by use of multidimensional scaling for breast masses on mammograms, Journal Digital Imaging, 11 Jaunuary, 2013 (online first).

[42] J.B.Kruskal : Multidimensional scaling, Beverly Hills, CA : Sage Publication, (1978).

[43] R.Yoshikawa, A.Teramoto, T.Matsubara, and H.Fujita: Detection of architectural distortion and analysis of mammary gland structure in mammograms using multiple Gabor filters, Medical Imaging Technology, Vol.30, No.5, pp.287-292, in Japanese, (2012).

[44] R.Yoshikawa, A.Teramoto, T.Matsubara, and H.Fujita: Preliminary study on the detection of the architectural distortion using adaptive Gabor filter, Proc. of International Forum on Medical Imaging in Asia, (2012).

[45] R.Yoshikawa, A.Teramoto, T.Matsubara, and H.Fujita: Automated detection scheme of architectural distortion in mammograms using adaptive Gabor filter, Proc. of SPIE Medical Imaging, in press, (2013).

[46] N.Yamada, T.Matsubara, A.Tsunomori, T.Hara, C.Muramatsu, T.Endo, and H.Fujita: Comparison of automated detection performance of architectural distortion on two kinds of mammograms, Proc. of International Forum on Medical Imaging in Asia 2012, 64, (2012).

[47] N.Yamada, T.Matsubara, A.Tsunomori, T.Hara, C.Muramatsu, T.Endo, and H.Fujita: Improvement of automated method for detecting architectural distortion using assessment of fibroglandular breast tissue density on mammograms, IEICE Technical Report, 112 (411), 89-94, in Japanese, (2013).

[48] Y.Okaniwa, K.Nishimura, C.Muramatsu, T.Hara, and H.Fujita: Study on improvement of the CAD system by the update of training data in clinical employment, JAMIT, (2012).

[49] C.Muramatsu, Q.Li, K.Suzuki, R.A.Schmidt, J.Shiraishi, G.M.Newstead, and K.Doi : Investigation of psychophysical similarity measure for evaluation of similar images for mammographic masses : preliminary results,"Medical Physics, Vol. 32, 2295-2304, (2005).

[50] M.Heath, K.Bowyer, D.Dopans, R.Moore, and P.Kegelmeyer, Jr : The digital database for screening mammography, Proc IWDM, 212-218, (2001).

[51] H.Nawa, T.Watanabe, D.Fukuoka, N.Terabayashi, T.Hara and H.Fujita: Development of image analysis and quantitative evaluation of the Locomotive syndrome, IEICE Technical Report, Vol.111, No.389, MI2011-133, 311-314, in Japanese, (2012).

[52] H.Nawa, T.Watanabe, D.Fukuoka, N.Terabayashi,, T.Hara and H.Fujita: Development of image analysis method for quantitative evaluation of the Locomotive syndrome, The Japanese Society of Medical Imaging Technology (Proc. of JAMIT2012), OP8-7, in Japanese, (2012).

[53] H.Nawa, T.Watanabe, D.Fukuoka, N.Terabayashi, T.Hara, and H.Fujita: 3D image analysis of gastrocnemius muscle for quantitative evaluation of the Locomotive syndrome, IEICE Technical Report, 112 (411), MI2012-75, 69-70, in Japanese, (2013).

[54] T.Furukawa, T.Kobayashi, S.Goshima, X.Zhang, X.Zhou, C.Muramatsu, T.Hara, H.Kondo, M.Kanematsu, and H.Fujita: Automatic extraction of liver contour for staging hepatic fibrosis on Gd-EOB-DTPA-enhanced MRI images, Proc. of International Forum on Medical Imaging in Asia, P1-3, (2012).

LIST OF ACCEPTED AND PUBLISHED PAPERS SINCE 1ST APRIL 2012

RELATED PEER REVIEWED PAPERS:

[1] C. Muramatsu, K. Nishimura, T. Endo, M. Oiwa, M. Shiraiwa, K. Doi, and H. Fujita : Representation of lesion similarity by use of multidimensional scaling for breast masses on mammograms, Journal Digital Imaging, 11 Jaunuary, 2013 (online first).

[2] C. Muramatsu, T. Matsumoto, T. Hatashi, T. Hara, A. Katsumata, X. Zhou, Y. Iida, M. Matsuoka, T. Wakisaka, and H. Fujita: Automated measurement of mandibular cortical width on dental panoramic radiographs, International Journal of Computer Assisted Radiology and Surgery, 23 Nov., 2012 (online first).

[3] A.Teramoto and H.Fujita: Fast lung nodule detection in chest CT images using cylindrical nodule-enhancement filter, International Journal of Computer Assisted Radiology and Surgery, June 2012 (online first).

[4] N.Kamiya, X.Zhou, H.Chen, C.Muramatsu, T.Hara, and H.Fujita: Model-based approach to recognize the rectus abdomens muscle in CT images, IEICE Transactions on Information and Systems, Vol.E-96-D, No.4, in press, (2013).

[5] T.Hara, M.Tagami, S.Mori, T.Kaneda, A.Katsumata, X.Zhou, C.Muramatsu, and H.Fujita, Automated detection of paranasal sinus diseases on dental panoramic X-ray image by using contralateral subtraction technique, IEICE Transactions on Information and Systems, Vol.J96-D, No.4., in press, in Japanese, (2013).

[6] C.Muramatsu, R.A.Schmidt, J.Shiraishi, T.Endo, H.Fujita, and K.Doi: Usefulness of presentation of similar images in the diagnosis of breast masses on mammograms: Comparison of observer performances in Japan and the USA, Radiological Physics and Technology, 6 (1), 70-77, (2013).

[7] H.Nagashima, K.Doi, T.Ogura, and H.Fujita: Automated adjustment of display conditions in brain MR images: Diffusion-weighted MRIs and apparent diffusion coefficient maps for hyperacute ischemic stroke, Radiological Physics and Technology, Vol.6, No. 1, 202-209, (2013).

[8] R.Yoshikawa, A.Teramoto, T.Matsubara, and H.Fujita: Detection of architectural distortion and analysis of mammary gland structure in mammograms using multiple Gabor filters, Medical Imaging Technology, Vol.30, No.5, pp.287-292, in Japanese (2012).

[9] A.Ikeya, A.Teramoto, T.Hara, and H.Fujita: Improving nodule detection in chest CT images using a cylindrical filter based on the anatomical structure of the lung, Medical Imaging Technology, Vol.30, No.5, pp.293-297, in Japanese (2012).

[10] Y.Uchiyama, T.Asano, H.Kato, T.Hara, M.Kanematsu, H.Hoshi, T.Iwama and H.Fujita: Computer-aided diagnosis for detection of lacunar infarcts on MR images: ROC analysis of radioloists' prformance, Journal of Digital Imaging, 25 (4), 497-503, (2012).

[11] N.Kamiya, H.Osaki, J.Kondo, H.Chen, and H.Fujita: Image interpretation system for informed consent to patients by use of a skeletal tracking, International Journal of Computer Technology and Applications, Vol.3, No. 4, 1593-1597, (2012).

[12] Y.Lee, D.-Y.Tsai, H.Hokari, Y.Minagawa, M.Tsurumaki, T.Hara and H. Fujita: Computerized detection of lung nodules by CT for radiologic technologists in preliminary screening, Radiological Physics and Technology, Vol.5, No.2, 123-128, (2012).

[13] T.Ohno, A.Teramoto, S.Suzuki, K.Ohara, M.Tsuzaka, and H.Fujita, "Preliminary study on a high-resolution breast CT: Development of experimental system and its evaluation," Medical Imaging and Information Sciences, Vol.29, No.2, pp.39-42, in Japanese (2012).

[14] X.Zhou, S.Wang, H.Chen, T.Hara, R.Yokoyama, M.Kanematsu, and H.Fujita: Automatic localization of solid organs on 3D CT images by a collaborative majority voting decision based on ensemble learning, Computerized Medical Imaging and Graphics, Vol.36, No.4, 304-313, (2012).

BOOKS, BOOK CHAPTERS AND REVIEWS:

[15] H.Fujita, T.Ishida, and S.Katsuragawa (eds.): Handbook of Practical Image Analysis in Medicine, Ohmsha, Tokyo, Japan, in Japanese, (2012).

[16] C.Muramatsu and H.Fujita: Detection of Eye Diseases, in Computer-aided Detection and Diagnosis in Medical Imaging, eds. by Q.Li and R.Nishikawa, Chap.19, in press, Taylor & Francis Books, Inc., (2013).

[17] Y.Uchiyama and H.Fujita: Detection of Cerebrovascular Diseases, in Computer-aided Detection and Diagnosis in Medical Imaging, eds. by Q.Li and R.Nishikawa, Chap.17, in press, Taylor & Francis Books, Inc., (2013).

[18] T.Hayashi, H.Chen, K.Miyamoto, X.Zhou, T.Hara, and H.Fujita: Computer-aided image analysis for vertebral anatomy on X-ray CT images (Chapter 7), ed. by K.Suzuki, in Computational Intelligence in Biomedical Imaging, in press, (2013).

[19] H.Chen, X.Zhou, H.Fujita, M.Onozuka, and K.Kubo: Age-related changes in trabecular and cortical bone microstructure, International Journal of Endocrinology, in press, (2013).

[20] H.Jiang, Z.Ma, M.Zong, H.Fujita, and X.Zhou: Abdomen CT image segmentation based on MRF and ribs fitting approach, Chapter 10, Lecture Notes in Electrical Engineering, Vol.206, 75-81, (2013).

INTERNATIONAL CONFERENCE PROCEEDINGS (WITH REVIEW):

[21] X.Zhou, A.Watanabea, X.Zhou, T.Hara, R.Yokoyama, M.Kanematsu, and H.Fujita: Automatic organ segmentation on torso CT images by using content-based image retrieval, Proc. of SPIE Medical Imaging, Vol.8314, 83143E-1 – 83143E-7, (2012).

[22] T.Hayashi, T.Matsumoto, T.Sawagashira, M.Tagami, A.Katsumata, Y.Hayashi, C.Muramatsu, X.Zhou, Y.Iida, M.Matsuoka, K.Katagi, and H.Fujita: A new screening pathway for identifying asymptomatic patients using dental panoramic radiographs, Proc. SPIE Medical Imaging, Vol.8315, 83152K-1 – 83152K-7, (2012).

[23] T.Matsumoto, T.Hayashi, T.Hara, A.Katsumata, C.Muramatsu, X.Zhou, Y.Iida, M.Matsuoka, K.Katagi, and H.Fujita: Automated scheme for measuring mandibular cortical thickness on dental panoramic radiographs for osteoporosis screening, Proc. SPIE Medical Imaging, Vol.8315, 83152L-1 – 83152L-6, (2012).

[24] A.Teramoto, H.Fujita, Y.Tomita, K.Takahashi, O.Yamamuro, and T.Tamaki: Pulmonary nodule detection in PET/CT images: Improved approach using combined nodule detection and hybrid FP reduction, Proc. SPIE Medical Imaging, Vol.8315, 83152V-1 – 83152V-6, (2012).

[25] M.Zhang, X.Zhou, S.Goshima, H.Chen, C.Muramatsu, T.Hara, R.Yokoyama, M.Kanematsu, and H.Fujita: An application to pulmonary emphysema classification based on model of texton learning by sparse representation, Proc. SPIE Medical Imaging, Vol.8315, 831534-1 – 831534-7, (2012).

[26] T.Matsumoto, T.Hara, J.Shiraishi, D.Fukuoka, H.Abe, M.Matsusako, A.Yamada, X.Zhou, and H.Fujita: User-friendly tools on hand-held devices for observer performance study, Proc. SPIE Medical Imaging, Vol.8318, 83181J-1 – 83181J-7, (2012).

[27] Y.Hatanaka, T.Inoue, S.Okumura, C.Muramatsu, and H.Fujita: Automated microaneurysm detection method based on double-ring filter and feature analysis in retinal fundus images, Proc. of the 25th International Symposium on Computer-Based Medical Systems, paper#150, (2012).

[28] C.Muramatsu, K.Nishimura, M.Oiwa, M.Shiraiwa, T.Endo, K.Doi, and H.Fujita: Correspondence among subjective and objective similarities and pathologic types of breast masses on digital mammography, Breast Imaging, A.D.A.Maidment, P.R.Bakic, and S.Gavenonis (Eds.), Proc. of 11the International Workshop, IWDM 2012, LNCS 7361, 450-457, Springer (2012).

[29] Y.Hatanaka, C.Muramatsu, A.Sawada, T.Hara, T.Yamamoto, and H.Fujita: Glaucoma risk assessment based on clinical data and automated nerve fiber layer defects detection, Proc. of the 34th Annual International Conference of the IEEE Engineering in Medicine and Biology Society (EMBC'12), 5963-5966, (2012).

[30] M.Zhang, X.Mou, H.Fujita, L.Zhang, X.Zhou, and W.Xue: Local binary pattern statistics feature for reduced reference image quality assessment, Proc. of SPIE Electronic Imaging, in press, (2013).

[31] X.Zhou, A.Yamaguti, X.Zhou, T.Hara, R.Yokoyam, M.Kanematsu, and H.Fujita: Automatic organ localizations on 3D CT images by using majority-voting of multiple 2D detections based on local binary patterns and Haar-like features, Proc. of SPIE Medical Imaging, in press, (2013).

[32] M.Zhang, X.Zhou, H.Chen, C.Muramatsu, T.Hara, R.Yokoyama, M.Kanematsu, and H.Fujita: Pulmonary emphysema classification based on an improved texton learning model by sparse representation, Proc. of SPIE Medical Imaging, in press, (2013).

[33] Y.Shimizu, T. Hara, D. Fukuoka, X.Zhou, C.Muramatsu, S.Ito, K.Hakozaki, S.Kumita, K.Ishihara, T.Katafuchi, and H.Fujita: Temporal subtraction system on torso FDG-PET scans based on statistical image analysis, Proc. of SPIE Medical Imaging, in press, (2013).

[34] A.Ikeya, A.Teramoto, K.Noguchi, and H.Fujita: Preliminary study on phase-contrast digital tomosynthesis: Development and evaluation of experimental system, Proc. of SPIE Medical Imaging, in press, (2013).

[35] R.Yoshikawa, A.Teramoto, T.Matsubara, and H.Fujita: Automated detection scheme of architectural distortion in mammograms using adaptive Gabor filter, Proc. of SPIE Medical Imaging, in press, (2013).

[36] C.Muramatsu, K.Nishimura, T.Hara, and H.Fujita: Preliminary investigation on CAD system update: Effect of selection of new cases on classifier performance, Proc. of SPIE Medical Imaging, in press, (2013).

[37] K.Nishimura, C.Muramatsu, M.Oiwa, M.Shiraiwa, T.Endob, K.Doi, and H. Fujita: Psychophysical similarity measure based on multi-dimensional scaling for retrieval of similar images of breast masses on mammograms, Proc. of SPIE Medical Imaging, in press, (2013).

[38] S.Mori, T.Hara, M.Tagami, C.Muramatsu, T.Kaneda, and A. Katsumata, H.Fujita: Automated detection of abnormalities in paranasal sinus on dental panoramic radiographs by using contralateral subtraction technique based on mandible contour, Proc. of SPIE Medical Imaging, in press, (2013).

CONFERENCE PROCEEDINGS (WITHOUT REVIEW):

[39] C. Muramatsu, Y. Hatanaka, A. Sawada, T. Yamamoto, and H. Fujita: Computerized analysis of glaucoma detection and staging by depth information and vessel routing in the disc on stereo retinal fundus images, Proc. of International Forum on Medical Imaging in Asia, 2012, 3 pages.

[40] A. Mizukami, C. Muramatsu, Y. Hatanaka, T. Hara, and H. Fujita: Improvement on extraction of low-contrast vessels for assessment of arteriolar narrowing on retinal fundus images, Proc. of International Forum on Medical Imaging in Asia, 2012, 4 pages.

[41] Y. Hatanaka, T. Inoue, S. Okumura, C. Muramatsu, and H. Fujita: Automated microaneurysms detection in retinal fundus images - Performance evaluation using ROC database -, IEICE Technical Report, 2013.

[42] M.Zhang, X.Zhou, S.Goshima, H.Chen, C.Muramatsu, T.Hara, R. Yokoyama, M.Kanematsu, and H.Fujita: Computer-aided diagnosis for pulmonary emphysema classification based on texton learning via sparse representation, Proc. of International Forum on Medical Imaging in Asia, 2012.

[43] S.Yamaguchi, X.Zhou, R.Xu, T.Hara, R.Yokoyama, M.Kanematsu, H.Hoshi, S.Kido, and H.Fujita: Construction of statistical shape models of organs in torso CT scans using MDL method, Proc. of International Forum on Medical Imaging in Asia, P2-33, 2012.

[44] Y. Uchiyama, T. Hara, J. Shiraishi, M.S. Chung, and H. Fujita: Improvement of CAD scheme for classification of lacunar infarcts and enlarged Virchow Robin spaces using Visible Korean Human Image, Proc. of International Forum on Medical Imaging in Asia, O5-2, 2012.

[45] A.Teramoto, H.Fujita, K.Takahashi, K.Ozaki, S.Murata, O.Yamamuro, T.Kobayashi, T.Tamaki, and M.Nishio, Development and evaluation of automated nodule detection in lung PET/CT images, Proc. of International Forum on Medical Imaging in Asia, 2012.

[46] A.Ikeya, A.Teramoto, K.Noguchi, and H.Fujita: Basic study on phase contrast imaging using micro-focus X-ray source and flat panel detector, Proc. of International Forum on Medical Imaging in Asia, 2012.

[47] R.Yoshikawa, A.Teramoto, T.Matsubara, and H.Fujita: Preliminary study on the detection of the architectural distortion using adaptive Gabor filter, Proc. of International Forum on Medical Imaging in Asia, 2012.

[48] C.Murata, A.Teramoto, and H.Fujita: Preliminary study on color optical CT: development of experimental system, Proc. of International Forum on Medical Imaging in Asia, 2012.

[49] T.Furukawa, T.Kobayashi, S.Goshima, X.Zhang, X.Zhou, C.Muramatsu, T.Hara, H.Kondo, M.Kanematsu, and H.Fujita: Automatic extraction of liver contour for staging hepatic fibrosis on Gd-EOB-DTPA-enhanced MRI images, Proc. of International Forum on Medical Imaging in Asia, P1-3, (2012).

[50] H.Nawa, T.Watanabe, D.Fukuoka, N.Terabayashi, T.Hara and H.Fujita,: 3D image analysis of gastrocnemius muscle for quantitative evaluation of the Locomotive syndrome, IEICE Technical Report, 112 (411), MI2012-75,69-70, in Japanese, (2013).

[51] N. Yamada, T. Matsubara, A. Tsunomori, T. Hara, C. Muramatsu, T. Endo, and H. Fujita: Improvement of automated method for detecting architectural distortion using assessment of fibroglandular breast tissue density on mammograms, IEICE Technical Report, 112 (411), 89-94, in Japanese, (2013).

Proceedings
of
the Fourth International Symposium
on
the Project "Computational Anatomy"

February 23 and 24, 2013

Venue: Icho Kaikan, Osaka University,
Osaka, JAPAN

Organizer
Coordination Committee of the Project "Computational Anatomy"